Integrated functions of microfluidics and gravimetric sensing enabled by piezoelectric driven microstructures

Jingui Qian[1], Yue Wang[1], Yuhang Xue[1], Habiba Begum[2], Yong-Qing Fu*[3], Joshua E.-Y. Lee*[4]

[1]Anhui Province Key Laboratory of Measuring Theory and Precision Instrument, School of Instrument Science and Opto-Electronics Engineering, Hefei University of Technology, Hefei, 230009, China
[2]Department of Electrical Engineering, City University of Hong Kong, Hong Kong, China
[3]Faculty of Engineering and Environment, Northumbria University, Newcastle upon Tyne, NE1 8ST, UK
[4]Centre for Audio, Acoustics and Vibration, University of Technology Sydney, Ultimo, NSW 2007, Australia

Correspondence and requests for materials should be addressed to J. E.-Y. Lee (joshua.lee@uts.edu.au) and Yong-Qing Fu (richard.fu@northumbria.ac.uk)

Abstract

Micro- and nano-electromechanical Systems resonators have been regarded as powerful tools for precision mass detection, and their abilities to measure these in a liquid environment open various opportunities for biosensing, chemical analysis, and environmental monitoring. Apart from overcoming issues of fluidic damping and electrical interfaces, there is a great challenge of bringing microanalytes to these devices with the required precision and scaling for high throughput sensing. Herein we address the above challenges by proposing a self-excited localized acoustic manipulation methodology based on a piezoelectric micromechanical diaphragm resonator (PMDR). Such the PMDR integrates acoustofluidics and mass sensing functions in tandem on a single device. Particle enrichment is realized within tens of seconds and the limit of detection is enhanced by mitigating common issues such as low capture rate and non-uniform distribution. The developed PMDR is versatile in its applicability to a range of particle sizes and densities for both acoustofluidic actuation and *in-situ* mass sensing. This work addresses long term technical challenges of inaccurate and inefficient measurement of liquid phase resonance mass sensing with great application potentials in biochemical detection and environmental monitoring.

Keywords: Acoustofluidics, piezoelectric resonators, liquid-phase mass sensing, Lamb waves, in-situ analysis

Introduction

The capability to detect rare microanalytes in a liquid environment is crucial for numerous applications across a broad spectrum of fields. For example, in the field of biology, monitoring the changes in cell mass or density during biological processes including its differentiation, apoptosis, and lesions could reveal its function and growth status, facilitating the pathological studies[1]. In the field of food safety, it is crucial to identify specific trace elements in wine production when monitoring the grape fermentation process[2]. In the field of chemical analysis, the ability to determine the concentration of harmful heavy metal pollutants in domestic and drinking water could protect human health[3]. In the field of environmental monitoring, detecting microplastics in the seawater could alleviate their long-term toxic effects on marine organisms[4]. Early studies were performed by immobilizing bioactive molecules on the surface of a quartz crystal microbalance (QCM) to form a recognition sensitive film, and then investigating relationship between mass loading and changes of resonance frequency for biological detection[5], mainly due to QCM's high quality factor and high frequency stability.

Micro- and nano-electromechanical (M/NEM) resonators for microanalyte detection have been widely investigated. These devices are typically processed by semiconductor fabrication techniques, which provide a high degree of manufacturing precision and enable miniaturization at a large production scale. By leveraging their low dimensional scales, M/NEM resonators have shown extraordinary sensitivities that stand-out from the QCMs, reaching attogram mass resolutions[6] or below. But in fluid environments, M/NEM resonators overarchingly face two inter-related problems of fluidic damping and electrical interfacing[7]. These challenges not only limit mass resolution and signal-to-noise ratio, but also cause the characteristic electrical signals to be undetectable. While it is possible to avoid the fluid environment and measure the device in air or vacuum by desiccating the sample to measure dry mass[8], the results do not provide the insights from real-time continuous monitoring. Through the implementation of more efficient electrical interfaces such as piezoelectric transduction[9] and engineering unique modes to minimize fluidic damping[10], much progress has been made to address these design-related bottlenecks[11][12][13].

Another challenge which has received less attention is to bring the analytes to the surface of the M/NEMS resonators, bearing in mind that droplet containing the sample (~ 2-3 mm in diameter) is typically much larger than the resonator. Various methods of micro-object manipulations have been reported, such as chemically modifying for

adsorption of micro-object[14][15], immobilizing bioactive molecules such as receptors, antibodies, DNA, and enzymes on the sensor surface to form a sensitive membrane[16], integrating dielectrophoresis (DEP) electrodes onto a resonant cantilever beam to capture micro-objects[17], or embedding a MEMS resonator into the microfluidic channel[18]. However, these methods have their limitations. For example, chemical adsorption, DEP manipulation and bio-sensitive membranes are applicable only for specific target microanalytes. Suspended resonant cantilevers embedded with microfluidic channels have been used to calibrate the buoyancy mass of the suspended cells, reaching femtogram level accuracy by operating the device in vacuum[19][20][21]. Other challenges include limited throughput by having to navigate through multiple channels when scaling to large arrays and requiring external pumps. The lack of a robust and scalable electrical readout method is another bottleneck for scale up[22][23]. In all cases, only a part of the total analytes interacted with the resonator inevitably. As such, the ability to bring close all the analytes present in the fluid to interact with the resonator would provide a notable boost to its sensitivity.

Among various manipulation techniques, acoustic tweezers have recently been shown as a label-free, non-contact manipulation tool for biology and analytical chemistry with exceptional dexterity[24][25]. In our recent attempt to bring acoustic tweezing methods to M/NEMS resonant sensors, we coupled the acoustic waves generated from a surface acoustic wave (SAW) device into a separate MEMS resonator chip. Randomly dispersed particles in a droplet were acoustically focused onto the MEMS resonator by micro-centrifugation, enabling nanogram mass measurement[26][27]. Notwithstanding, micro-centrifugation is limited to one target site per chip. Thus, even though microfabrication of arrays of MEMS resonators allows for multiplexed sensing, this limitation of micro-centrifugation presents a bottleneck for scaling up throughput on a single chip. As such, highly localized and scalable particle manipulation techniques that are truly compatible with MEMS resonators are lacking.

Recent studies by Cheng et al. and Vachon et al. have demonstrated the generation of guided waves on a chip using transversely vibrating microfabricated diaphragms[28][29] to enable highly localized particle control in a fluid. As such, these results imply the possibility to collocate the fluidic actuator with the resonant sensor on the same substrate/chip. By considering the mode of vibration, herein, we demonstrate that the same transversely vibrating microfabricated diaphragm provides both the fluidic actuator and resonant sensor. Such the microfabricated diaphragm is based on a piezoelectric micromechanical diaphragm resonator (PMDR) driven to oscillate in a higher order transverse mode. By actuating the PMDR at a higher voltage (12-24 V_{pp}), randomly dispersed micro-objects inside the droplet were trapped around the anti-nodes

of the vibration mode. Then by decreasing the voltage (0.7 V_{pp}) and using the same vibration mode for sensing, the trapped particles from the actuation phase are conveniently coincident with the most sensitive spatial regions, benefiting accurate mass sensing. The interaction between micro-objects and the PMDR can be monitored through the shift in the device's resonant frequency in liquid.

We further studied acoustic enrichment effects and the durations of a single cycle with particles of different diameters and densities under various excitation input power levels. The differences in shifts of resonant frequencies between sparsely distributed particles and acoustically focused particles reveal the importance of acoustic localization for highly sensitive detection. Using the PMDR, we demonstrated concentration identification and density classification as a prospective *in-situ* analysis tool. We believe that the developed PMDR holds great potential applications in the fields of biological detection, chemical analysis, food detection, environmental monitoring.

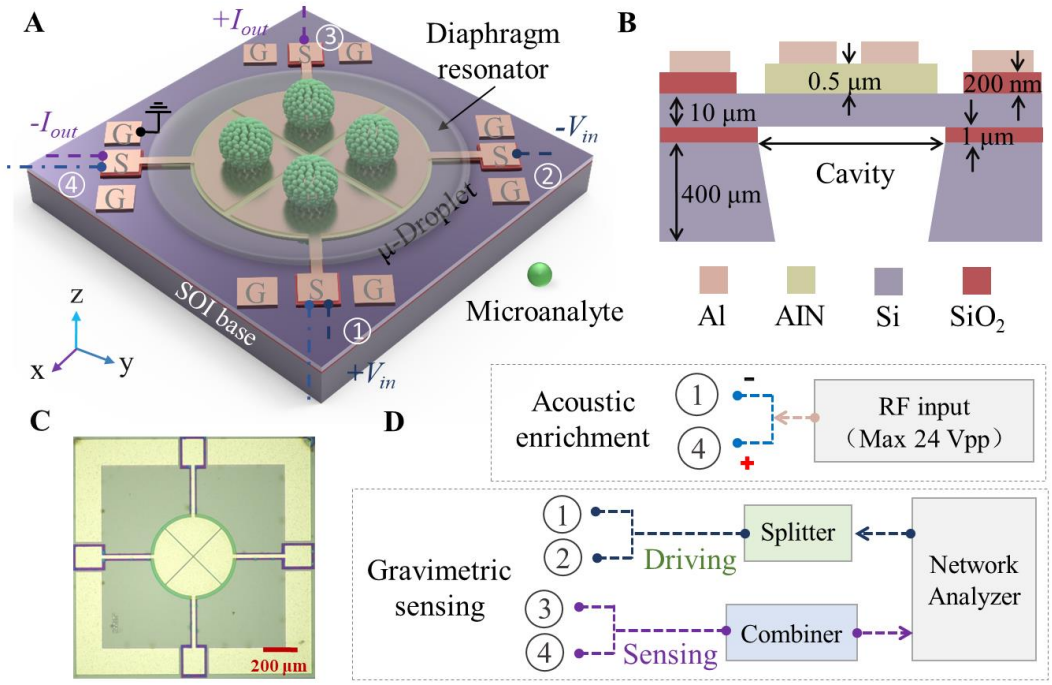

Fig. 1 Design, fabrication and work principle of the PMDR. (A) Schematic diagram showing a perspective view of the PMDR and working principle for acoustic manipulation and liquid-phase mass sensing of micro-objects by actuating the transverse (2, 0) resonant mode. (B) Side view schematic of the PMDR showing the various layers including the electrode, piezoelectric film and etched cavity, which defines the clamped boundary of the free-standing diaphragm. (C) Top view of the PMDR under an optical microscope. (D) Electrical connection of acoustic enrichment and gravimetric sensing (fully differential configuration).

Results and Discussion

Structure design and work principle of PMDR.

We proposed a fully anchored diaphragm structure to fully seal the top of the device from the bottom cavity (**Fig. 1**) to meet the structural requirements of micro-resonant devices in acoustofluidics. This design effectively prevents any potential leakage of sample droplets, loaded on the top side of the diaphragm, during acoustic manipulation. As illustrated in **Fig. 1(A)**, the proposed PMDR is comprised of four 90-degree sector electrodes which are excited to generate the transverse (2,0) resonance mode[30]. **Fig. 1(B)** shows a cutaway view of multilayer structure of the PMDR, including a 400 μm thick silicon substrate, 1 μm thick buried oxide layer, 10 μm thick silicon device layer (n-doped top layer to create an Ohmic contact with the deposited 1 μm thick top Al electrode, acting as the bottom electrode), 0.2 μm thick SiO_2 layer, and 0.5 μm thick AlN piezoelectric thin film. An optical microscope of the fabricated PMDR is shown in **Fig. 1(C)**. The electrode contact pad is designed in the form of ground-signal-ground (GSG) to reduce the parasitic feedthrough effect. Typically, there is a slight beveling of the sidewalls with roughly a 30 μm over-extension when the backside cavity is etched to create a nearly trapezoidal cavity. A microliter liquid sample (i.e., about 2 μL) containing microanalytes is placed on the PMDR surface forming a droplet with a diameter of about 1 mm as the electrode surface is naturally hydrophobic (**supplementary information S1**).

When performing acoustofluidic particle manipulation, the piezoelectric transducer allows the effective conversion of input RF signals (12-24 V_{pp} applied around the resonance frequency of the PMDR in liquid) into output acoustic waves by actuating the diaphragm to resonate in the transverse (2,0) mode. Here, two adjacent sector electrodes are driven by the RF signals (e.g., using DC probes to the respective signal pads) with a signal generator shown in **Fig. 1(D)**. The highly localized acoustic waves generated directly interact with the micro-droplet on the PMDR, minimizing energy attenuation associated with long-distance propagation of acoustic waves in the liquid medium as in the case of SAW devices.

To measure the resonance frequency of the PMDR, the swept frequency response of the PMDR is obtained through the driving and sensing all four electrical ports differentially using the GSG probes. We input RF signals via differential voltages ($+V_{in}$ and $-V_{in}$) to drive one pair of adjacent sector electrodes. The driving electrodes generate anti-phase mechanical strains because of the reverse piezoelectric effect. Meanwhile, the other adjacent two electrodes generate the opposing field polarities in response to the

associated mechanical strains governed by the direct piezoelectric effect. The opposing polarization fields are sensed as the differential currents (i.e., $+I_{out}$ and $-I_{out}$). **Fig. S2 (**in the **supplementary information)** shows the series resonant RLC equivalent circuit model with the parasitic feedthrough elements which represents the electromechanical response of PMDR. **Fig. 1(A)** and **Fig. 1(D)** show the fully differential configuration (i.e., power splitting with a 180° phase shift applied to both the input and output ports) to reduce the parasitic feedthrough of the RF signals and enhance electrical characterization in the liquid phase when measuring the resonance. Feedthrough generally plagues all the electrical measurements of resonators in a liquid environment. There are various mitigation methods which are outlined in **supplementary information S3**. The fully differential (including differential input and differential output) configuration provides a two-stage feedthrough cancellation scheme, whereby any remnant feedthrough after the differential input stage is further reduced when summed differentially at the outputs[30][31]. This allows for feedthrough cancellation via differential signals within a single device without invoking a second unreleased twin structure.

The PMDR with a diameter of 560 μm shows a high quality factor (Q) of 211 and a low dynamic (i.e. motional) resistance (R_m) in the liquid phase[30]. Finite element analysis (FEA) simulations were performed using the commercial software of COMSOL 6.0 based on a diaphragm radius of 280 μm, after accounting for a 30 μm over-extension of the cavity from the backside etch in the fabrication. The simulated quarter-section view of the deformation profile and the corresponding lateral strain profile of the (2, 0) resonant mode are shown in **Fig. 2(A).** The generated acoustic pressure field distribution within a modelled sessile droplet (e.g., with a height of 300 μm and a radius of 500 μm) is shown in **Fig. 2(B),** for a given phase of the generated wave, inverting in the next half cycle of oscillation.

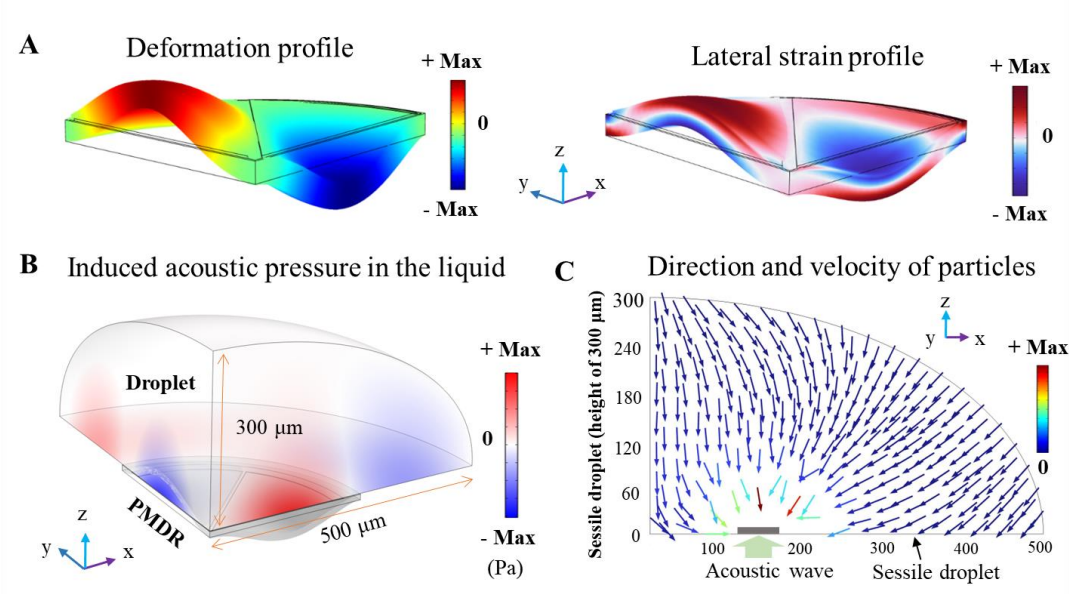

Fig. 2 Theoretical simulation of the PMDR resonance for acoustic enrichment and mass sensing. (A). Simulation of the deformation profile and lateral strain profile of the transverse (2, 0) mode excited in a circular diaphragm with the diameter of 560 μm. (B) Sectional view of the induced acoustic pressure by the resonance of PMDR in a sessile droplet. (C) Particle trace simulation model shows the direction and velocity of particles in a droplet under the treatment of acoustic radiation force (applied at the position of the bold grey line), while the trajectory of particles is animated in **Video S1** (Multimedia available online).

To mimic the particle trajectories under the actuation of localized acoustic waves within a droplet, we established a simple axisymmetric model (**Fig. 2(C)** and **supplementary material Video S1**) in the X-Z plane corresponding to **Fig. 2(B)**. In the axisymmetric model, to simulate the acoustic radiation forces arising from the deformation of the underlying diaphragm resonating in the transverse (2,0) mode, we applied a z-direction wave radiation at the bottom droplet boundary. The radiation wave was applied within the interval corresponding to a non-zero diaphragm deformation (> 90% of the maximum amplitude). More specifically, the radiation wave was applied between 127-177 μm from the origin center of droplet (indicated by the bold grey line in **Fig. 2(C)**). The direction of each arrow indicates the direction of the particle motion, while its color denotes the corresponding velocity magnitude. A simulated animation of particle enrichment trajectories under the acoustic treatment is provided in the **supplementary material Video S1**. The patterns of the arrows show that the particles are clustered and localized (with the reference to **Fig. 2(C)**) at the positions of highest acoustic pressure (with the reference to **Fig. 2(B)**).

Generally, resonators can be simplified into a mass-damper-spring mechanical

resonance system. The resonance frequency of the transverse (2,0) mode PMDR is given by the equation (1):

$$f_0 = \frac{1}{2\pi}\sqrt{\frac{k}{m}} \quad (1)$$

where m denotes the dynamic mass, and k denotes the spring constant[32]. By inputting the RF signals with the resonant frequency to excite transverse flexure mode in this case, the acoustic pressure field is generated on the diaphragm to induce formation of gradient forces inside the droplet and move the microanalyte. The acoustic radiation force drives the particles towards the center region of each sector electrode (e.g., the highest displacement), pulling the particles down to the surface of the diaphragm as visualized by **Fig. 2(C)**. This is an inherent feature of acoustofluidic enrichment that broadly applies across different acoustic tweezing devices (e.g., SAW[33], CMUT[34], PMUT[28], SAW coupled to silicon[35], and SAW coupled to TPoS[26]). We have selected particle materials that are denser than water (i.e. the medium containing the different particles), such that their inertia is greater than the buoyancy. Furthermore, intermolecular attractive forces (e.g., electrostatic, capillary, and van der Waals forces) further induce further surface adhesion[36][37], ensuring that the particle clusters remain attached to the surface of the electrodes of the PMDR even after acoustic waves have been switched off. The resulting loading on the PMDR causes the downshift of the resonant frequency of the PMDR.

Characterization of acoustofluidics on the PMDR.

Fig. 1(A) shows the liquid-phase electrical characteristics of the transverse (2,0) mode diaphragm resonator. The MEMS chip was mounted on the probe station and electrically connected to a network analyzer (with an internal RF signal of 10 dBm) using four G-S-G probes. The electrical transmission signals (S_{21}) of the PMDR with different diameters were measured. Results show that the resonant frequency of the PMDR in the water is much lower than that in air (**supplementary information S4**). The PMDR with a diameter of 560 μm shows the strongest resonant peak as it has the lowest R_m and highest Q values as shown in **S5 (supplementary information**). It is worth noting that all these measurement results in the liquid phase show a higher Q factors compared to those in air. A detailed discussion of the above phenomenon is provided in the **supplementary information S6**.

Figs. 3(C-F) show the particles' enrichment results induced by self-excited Lamb wave generated from the PMDR resonance, in which the diameters of PMDR (e.g., 560 μm, 660 μm, 760 μm and 860 μm) show no apparent effect on the performance of acoustofluidic concentration. The covered area from the micro-liter droplet is typically larger than that of the diaphragm area (or the resonant sensing area). The microanalyte

associated particles are sparsely dispersed in the initial state. However, they are quickly focused onto the sensing area and adhered to the electrode surface under the internal gradient force induced by the acoustic pressure field from the transverse flexure diaphragm. Instead of being uniformly distributed all over the entire diaphragm, the focused particles form four major clusters when viewed from the top, which matches well with the transverse (2, 0) resonant displacement profile of the PMDR. This phenomenon is exactly opposite to what has been typically observed in the SAW device manipulation. The underlying mechanism for acoustofluidic actuation based on micromachined structures is discussed in the **supplementary information S7**.

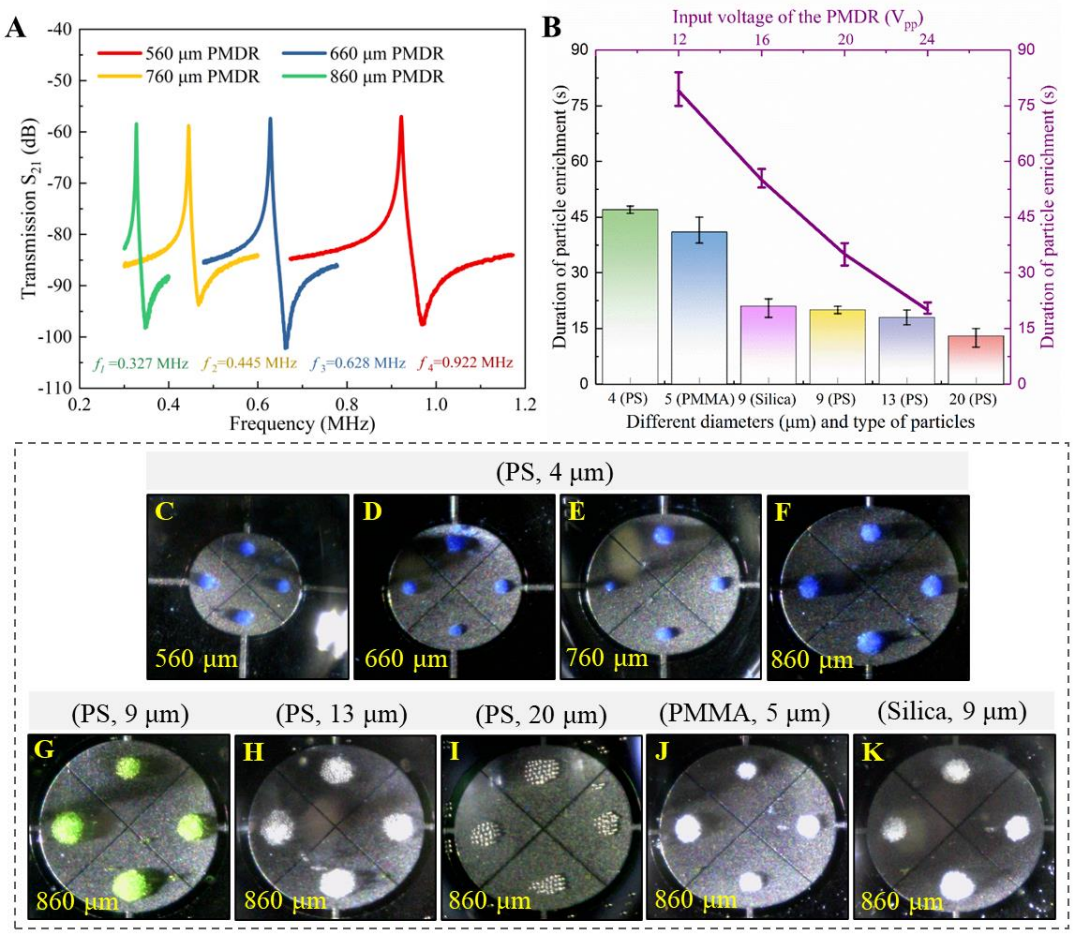

Fig. 3 Performance characterization of acoustofluidics enabled by PMDR. (A). Electrical transmission measurements of PMDRs with different diameters characterized in liquid phase. (B). Duration of acoustic enrichment at various input voltages (12 V-24 V) acting on different diameters (4-20 μm) and types of particles using the 860 μm-diameter PMDR (346.75 kHz). (C-F). Demonstration of acoustic particle enrichment actuated by PMDRs of different diameters (Multimedia available online). (G-K). Demonstration of acoustic enrichment with different diameters and type of particles using the 860 μm-diameter PMDR (Multimedia available online). Dyed particles were diluted in DI water to obtain the same concentration of 0.375 mg/mL.

The duration required for particle enrichment completion was identified as one of the key qualitative evaluation criteria for the acoustofluidic effect of the PMDR. The enrichment process is regarded as completed once there are no more moving particles and the size of cluster centered on each top no longer changed visibly. As shown in **Fig. 3(B)**, the durations of particle enrichment are inversely proportional to the input voltage and also to the particle diameters, when using the same 860 μm-diameter PMDR and different types of particles. The results of particle enrichment patterns of different types of particles generated on the PMDR at $24V_{pp}$ are shown in **Figs. 3(G-K)**. They all show well-formed patterns of accumulated particles of different sizes and different densities. For example, using 9 μm PS particles, the acoustic enrichment time was shortened from 79 s to 20 s when the input voltage was increased from 12 V_{pp} to 24 V_{pp}. In terms of particle size effects, for the same input voltage of 24 V_{pp}, the acoustic enrichment time was about 47 s for the 4 μm-diameter PS particles but reduced to 13 s for 20 μm-diameter PS particles. Meanwhile, the acoustic enrichment durations for the higher density particles (e.g., silica) are slightly longer than those of lower density particles (e.g., PS). The results of acoustic enrichment and concentration of particles of different sizes and types using the PMDR with a diameter of 860 μm are shown in the **supplementary material Video S2** (Multimedia available online). It is worth noting that the acoustically enriched particle size should be larger than or at least equal to 4 μm.

As demonstrated in **supplementary information S8**, we discovered an alternative electrical driving method, in which the RF signal was connected to one single sector electrode (i.e., using DC probes) with signal pad and ground pad, and circumferential propagation of Lamb waves excited the transverse (2,0) mode of the PMDR. However, it takes longer to enrich particles when driving a single electrode compared with driving two adjacent sectors.

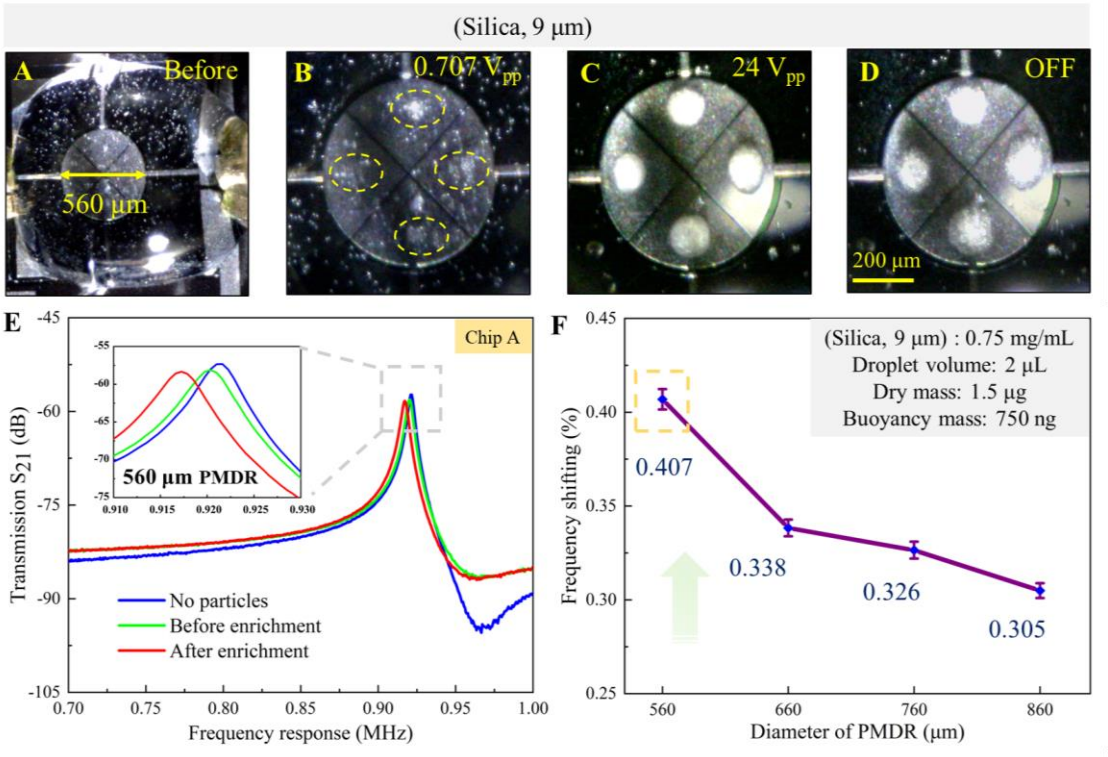

Fig. 4 Acoustofluidic-assisted liquid-phase mass sensing by the PMDR. (A-D). Complete sequence of acoustic particle (9 μm silica particles) enrichment from initiation to deactivation using chip A. (A) The droplet of 2 μL was placed on the surface of the PMDR with a diameter of 560 μm, and the particles inside the droplet were sparsely dispersed everywhere. (B) When measuring the electrical transmission (S_{21}) of the PMDR, only a few particles moved slightly to show a tendency to enrichment. (Multimedia available online) (C) When performing the acoustofluidic experiment with 24 V RF signal, all the particles were enriched to form four clusters to match the resonance modes. (D) The acoustically focused particle cluster remained intact after turning off the RF signal. (E) Electrical transmission (S_{21}) of the PMDR in three conditions, DI water without particles, DI water with sparse particles and DI water with acoustic focused particles. (F) Frequency shift from before and after the acoustic particle enrichment for different diameters of PMDRs using the same particle sample conditions (silica particles with a concentration of 0.75 mg/mL). Labeled values refer to the mean of repeated readings recorded ($N \geqslant 3$) while the error bars refer to the maximum and minimum values recorded.

Demonstration of liquid-phase mass sensing of PMDR.

Three PMDR devices on separate dies (named chips A, B, C, with the same parameters) were selected to demonstrate integrated acoustic actuation and mass sensing of particles on the same batch of micromechanical device. **Figs. 4(A-D)** show the entire sequences of acoustic particle enrichment using the chip A. The self-excited Lamb wave generated by the PMDR drives the particles inside the droplet to rapidly accumulate in the four most sensitive regions to form four compact clusters under an input voltage of 24 V.

After turning off the RF signals, the particle clusters are maintained in their initially trapped positions. As such, the acoustofluidic localized particle cluster pattern will still be at the maximum sensitivity regions of the PMDR for the next step (i.e., resonant sensing of the particle cluster in the liquid phase). This new methodology solves the common problem of uncertainty and uneven distribution of microanalytes loaded on the resonator during the detection of low-concentration samples. At low concentrations, unfocused particles inevitably lead to blank measurement results caused by no particle loaded and notable measurement errors caused by random distribution.

To investigate interferences of the frequency response measurement experiment on acoustofluidic manipulation, we characterized the particles' motions when the PMDR device was driven by the network analyzer. When a voltage of 0.7 V_{pp} (i.e., or 10 dBm and 0.4 V_{rms}) was applied to the two adjacent actuation electrodes, only a few particles were moved and only just slightly. There is no indication of particle delocalization and enrichment as shown in the **supplementary material Video S3** (Multimedia available online). Therefore, we confirm that the swept frequency response measurement experiment has no effect on acoustofluidic manipulation. As plotted in **Fig. S5**, to analyze the measurement uncertainty, we performed multiple frequency sweep measurements over 5-6 minutes for PS particles, which shows the lowest density and thus the highest probability of delocalization over time. The results show that the resonant frequency has not been changed for the first 3 min and only begins to change after 5 min (possibly indicating onset of delocalization). However, we should address that 3 min is ample for multiple measurements.

The electrical transmission (S_{21}) signals in the following three conditions are plotted in **Fig. 4(E)**, i.e., in DI water without particles, DI water with sparse particles, and DI water with acoustic focused particles, respectively. The analytical equation for the resonant frequency shows that the resonant frequency is inversely proportional to the square root of the dynamic mass. The experimental results are consistent with the theoretical analysis, as observed from the down shift in the resonant frequency of the PMDR due to the mass loading effect. It should be noted that the fractional frequency shift after focusing particles (0.407% relative to only DI water on the PMDR) is much larger than that when the sparse particles are unfocused (0.068%). We have performed repeated resonance frequency sweep measurements both before and after enrichment process (i.e., triplicates in each case). In the case of **Fig. 4(F)**, the volume of the μ-droplet was 2 μL and the concentration of the silica particles in the μ-droplet was estimated to be 0.75 mg/mL. The dry and buoyant masses, calculated from the equations in supplementary information **S10,** were 1.5 μg and 750 ng, respectively. Accordingly, the loading mass of 750 ng was calibrated based on the measured

fractional frequency shift of 0.407% for the 560 μm diameter PMDR as well as the shift of 0.305% for the 860 μm PMDR. Specifically, the 560 μm-diameter PMDR demonstrated the largest fractional frequency shift among the different diameters of PMDRs tested as shown in **Fig. 4(F)**, in which the magnitude of resonant frequency shift was decreased monotonically with increasing the resonator diameter.

While the position dependence of the resonant frequency is well-documented for single particles[38], we have not found this to be the case here. Despite the clear differences in the cluster distribution, the corresponding variation in the resonant frequency is nearly indistinguishable compared to the resonant frequency prior to the localization (see the supplementary information **S11).** In brief, based on the above results, we have verified the feasibility of calibrating the loading mass of the enriched particles based on the measured resonance frequency offset before and after the acoustofluidic actuation.

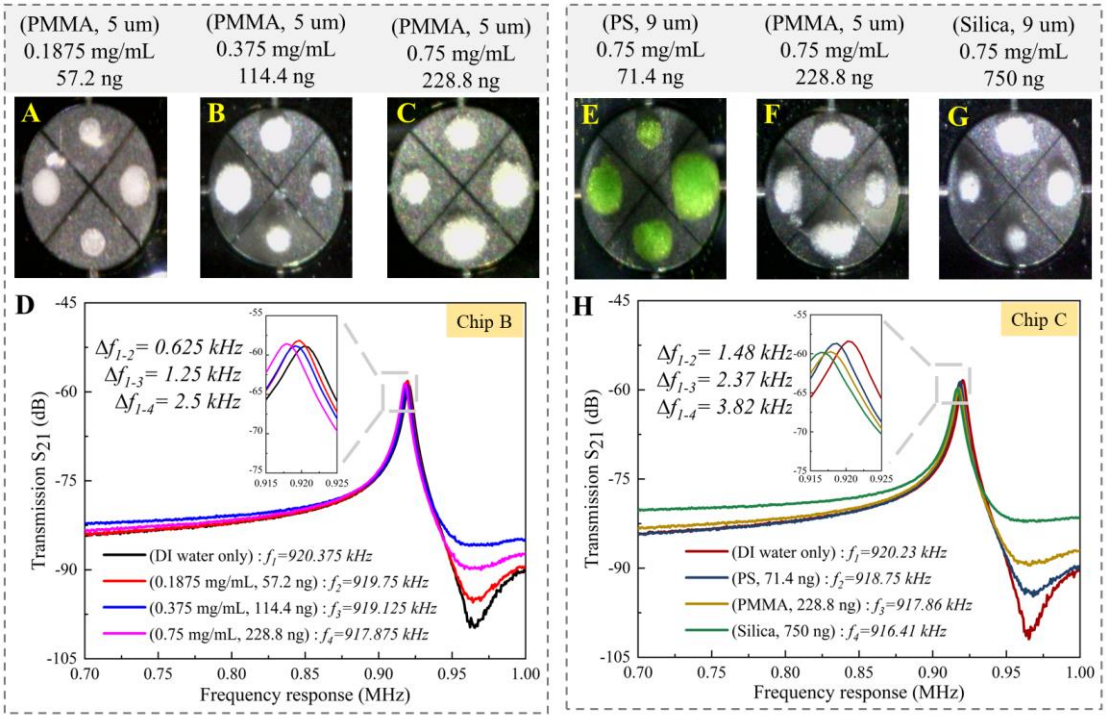

Fig. 5 Demonstration of the PMDR for concentration measurement and density identification of micoanalyte. (A-C). Results of acoustic enrichment with different concentrations (0.1875 mg/mL, 0.375 mg/mL, 0.75 mg/mL) of PMMA particles using chip B. (D). Electrical transmission (S_{21}) of the PMDR capturing the increase in frequency shift with the increase in particle (PMMA) concentration added. (E-G). Results of acoustic enrichment with the same concentration (0.75 mg/mL) of PS particles, PMMA particles and silica particles using chip C. (H). Electrical transmission (S_{21}) of the PMDR capturing the increase in frequency shift with the increase in particle mass density (using different particle materials) added at the same concentration.

Identification of micoanalyte concentration and density using PMDR

We further demonstrated the potential applications of the PMDR in measuring and identifying the concentrations and types of microanalytes (e.g., their densities). As shown in **Fig. 5** and **supplementary information S12**, the frequency shift was positively correlated with particle concentration for the same particle type and the particle material densities at the same concentration. Therefore, the direct relationship between the frequency shift of the PMDR and the loaded mass (i.e., the focused particles in the micro-droplet) could be identified. As shown in **Figs. 5(A-D)**, the PMMA particles with different concentrations (i.e., 0.1875 mg/mL, 0.375 mg/mL, and 0.75 mg/mL) are distinctly clustered at each of the four sectors on the PMDR surface. The respective loading buoyant mass values (i.e., 57.2 ng, 114.4 ng, 228.8 ng) are corresponding well to the resulting frequency shifts of 0.625 kHz, 1.25 kHz, 2.25 kHz (or 0.068%, 0.1136%, 0.272%), respectively. As shown in **Figs. 5(E-H)**, various types of particle samples (e.g., PS particles, PMMA particles and silica particles) with the same concentration (0.75 mg/mL) are all distinctly clustered in each of the four sectors on the PMDR surface. Similarly, the respective loading buoyant mass values (71.4 ng, 228.8 ng, 750 ng) are corresponding well to the resulting frequency shifts of 1.48 kHz, 2.37 kHz, 3.82 kHz (or 0.161%, 0.258%, 0.415%), respectively. All the extracted parameters for the Chips A, B and C prior to adding the particles and after acoustically focusing particles of different types or densities are summarized in the **supplementary information S13**.

We further embedded the PMDR in a phase-locked loop (PLL) for self-oscillation, to demonstrate the possibility of the PMDR to be efficiently implemented in a close loop to track the frequency in real-time for liquid-phase sensing applications. As depicted in **Fig. 6**, the PMDR can be locked into oscillation under two conditions, i.e., (1) in the pure water droplet, or (2) in the droplet with enriched particle clusters. To evaluate stability, reliability and accuracy of measured frequency shifts caused by the loaded buoyant masses of particle samples, we recorded the oscillation frequencies over a period of 5 min at a sampling time of 1.16 ms. The results shown in **Fig. 6(A)** demonstrate that the frequency noise and drift over time are much smaller than the frequency shift detected after focusing the particles. The Allan deviation[39] of the frequency outputs in a short time window of 100 seconds was also calculated (e.g., by normalizing the values over the respective resonant frequencies). The results show that the minimum Allan deviation was 1.9 ppm at 0.5 s. With a minimum frequency shift of 1.7 Hz calculated from the Allan deviation, the PLL-operated PMDR reaches an equivalent limit of detection (LOD) of approximately 1.03 ng/μL (all the detailed calculations are provided in **supplementary information S14**). The LOD value of the

PMDR is comparable well with those reported in other literatures[40][41], and meet the requirements of mass analysis of ultra-low concentration particle samples. The shape of the Allan deviation curves indicates that the frequency stability is dominated by temperature-related frequency drift as no temperature compensation was applied in the measurement setup.

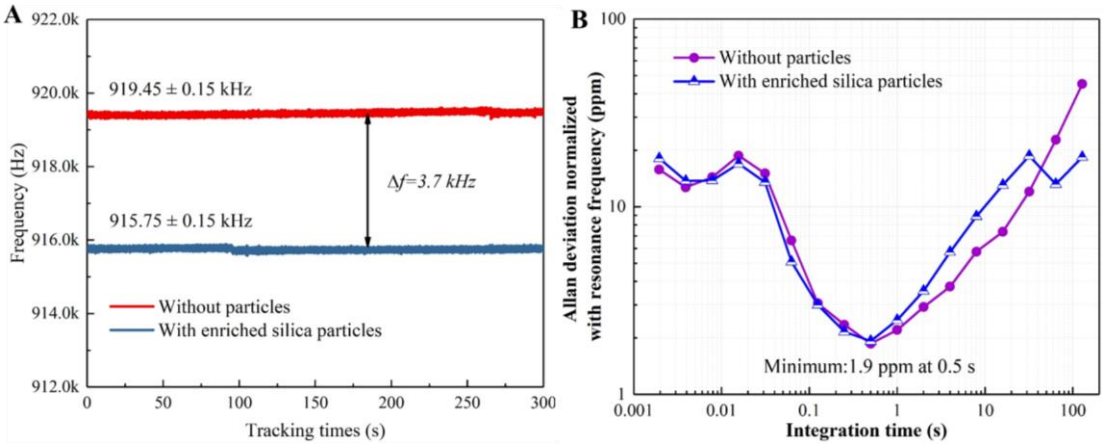

Fig. 6 Embedding the PMDR in a phase-locked loop for self-oscillation towards real-time sensing applications. (A). The PMDR were locked into oscillation for long-term frequency tracking without particles and with enriched silica particles (B). The corresponding Allan deviation normalized with resonance frequency during the integration time.

The merits of the proposed PMDR to integrated acoustofluidic manipulation and mass sensing for microanalyte detection are highlighted in the **supplementary information S15**. Among various particle localization techniques, the PMDR enabled acoustofluidic device presents excellent particle enrichment outcomes in the shortest time. It is compatible with a wide range of sizes and densities of microparticles, and reusable after rinsing with DI water. However, the damping of the transverse (2,0) mode in the liquid could significantly affect the resolution of the mass measurement. Tao et al. previously proposed a hybrid mode, i.e., fluidic actuation using Lamb waves and biosensing using the thickness shear waves[42] on a conventional cm-scale SAW device substrate. As such, the next line of innovation would be designing novel structures that incorporate two different modes in a micromechanical resonator, i.e., one mode favoring acoustic actuation and the other mode favoring resonant sensing[43].

Conclusion

In conclusion, this work verifies that the self-excited acoustofluidic localization effect on the PMDR drives the rapid accumulation of microanalytes in mass sensitive regions of the PMDR within a droplet. This greatly enhance nanogram-scale liquid phase mass

sensing, which is a breakthrough solution that addresses issues of trapping failure, measurement inaccuracy, and low accuracy in liquid phase resonance mass sensing. The PMDR with a diameter of 560 μm was well able to acoustically manipulate a wide range microparticles (4-20 μm) in addition to high sensitivity for mass sensing of microanalytes. The loaded buoyancy mass of the enriched particles with different concentrations and types was directly calibrated by the resonance frequency shift before and after acoustic localization. The stability, reliability and accuracy of the mass sensing were confirmed by embedding the PMDR in a real-time phase-locked loop for self-sustained oscillation. The proposed PMDR holds promise as a scalable compact integrated solution to benefit the field of rapid disease diagnosis, food production processes, and environmental pollution monitoring.

Experimental Section

A. Fabrication of the PMDR. The PMDR was fabricated by MEMSCAP® using the standard PiezoMUMPs process[44], which was started with a silicon-on-insulator (SOI) wafer including of a 400 μm thick silicon substrate, one μm thick buried oxide layer, and 10 μm thick silicon device layer. Firstly, a 0.2 μm thick SiO_2 layer was thermally grown on the SOI wafer and etched using the reactive ion etching (RIE) process to form a designed pattern. Secondly, a 0.5 μm thick AlN layer was deposited using the magnetron sputtering and patterned by wet etching. Next, a Cr/Al (20 nm/1000 nm) metal layer was deposited and then patterned to form the contact pad and electrodes. Finally, a backside cavity was etched using a deep-RIE (DRIE) process after using hydrofluoric acid-based etching of the buried oxide layer to release the diaphragm structure defined by the silicon device layer.

B. Sample preparation. Solutions of commercial PS particles (ρ=1.05 g/cm^3, DaE Scientific, China) with different diameters (4 μm, 9 μm, 13 μm, 20 μm), PMMA particles (ρ=1.15 g/cm^3, DaE Scientific, China) and silica particles (ρ=2 g/cm^3, DaE Scientific, China) were diluted into deionized (DI) water in a certain proportion.

C. Experimental setup and measurement system. A vector signal generator (FY6900, FeelElec, China) was firstly applied the RF signals to the PMDR for performing acoustofluidic experiments. Then a network analyzer (Agilent E5061A, USA) was used for the frequency response measurement. The MEMS chip with the PMDR device was mounted on a probe station (C-2, EVERBEING, Taiwan) for electrical connection with the GSG probes. A digital microscope (AM7515MZTL, Dino-Lite, Taiwan) was assembled on the probe station for observation and recording of acoustofluidic behavior.

A fully differential driving and sensing connection of PMDR was enabled by two RF power splitters (Mini Circuits ZFSCJ-2-1-S+, 1-500 MHz). A sample droplet of microanalyte (approximately 2 μL) was pipetted (JOAN LAB, 10 μL, China) on top of the PMDR. The oscillation frequency of PMDR was measured using a digitally configurable phase-locked loop (UHF LI, Zurich Instruments). The contact angle of a DI water droplet of 2 μL was measured using a droplet shape analyzer (OCA 15EC, Dataphysics, Germany).

SUPPLEMENTARY MATERIAL

See the additional detailed experimental data and demonstration videos to support the conclusions of the main manuscript.

ACKNOWLEDGMENTS

This work was supported by the National Natural Science Foundation of China (Grant No. 62301209), the Natural Science Foundation of Anhui Province (Grant No. 2308085QF196), the Fundamental Research Funds for the Central Universities (Grant No. JZ2024HGTB0243), and the Hong Kong Research Grants Council under Project CityU 11218118.

AUTHOR DECLARATIONS

Conflict of Interest Statement

The authors have no conflicts to disclose.

Author Contributions

J. Qian and J. E.-Y. Lee conceived the research. J. Qian and Y. Wang performed the research. H. Begum and J. Qian designed the device. Y. Xue commit to drawing. J. Qian and Y. Wang wrote the manuscript. J. E.-Y. Lee and Y.-Q. Fu analysed data and revised the manuscript.

DATA AVAILABILITY

The data that support the findings of this study are available within the article and its supplementary material.

REFERENCES

[1] L. Mu, J. H. Kang, S. Olcum, K. R. Payer, N. L. Calistri, R. J. Kimmerling, S. R. Manalis, T. P Miettinen, Mass measurements during lymphocytic leukemia cell polyploidization decouple cell cycle and cell size-dependent growth, PNAS, 117, 15659-15665 (2020).

[2] J. Toledo, V. Ruiz-Díez, G. Pfusterschmied, U. Schmid, J. L. Sánchez-Rojas, Flow-through sensor based on piezoelectric MEMS resonator for the in-line monitoring

of wine fermentation, Sens. Actuator B: Chem., 254, 291-298 (2018).
[3] N. Wang, E. Kanhere, M. S. Triantafyllou, J. M. Miao, Shark-inspired MEMS chemical sensor with epithelium-like micropillar electrode array for lead detection, 2015 18th International Conference on Solid-State Sensors, Actuators and Microsystems (TRANSDUCERS), 1464-1467 (2015).
[4] H. S. Auta, C. U. Emenike, S. H. Fauziah, Distribution and importance of microplastics in the marine environment: a review of the sources, fate, effects, and potential solutions, Environ. Int., 102, 165-176 (2017).
[5] I. Mannelli, M. Minunni, S. Tombelli, M. Mascini, Quartz crystal microbalance (QCM) affinity biosensor for genetically modified organisms (GMOs) detection, Biosen. Bioelectro., 18, 129-140 (2003).
[6] E. Sage, M. Sansa, S. Fostner, et al., Single-particle mass spectrometry with arrays of frequency-addressed nanomechanical resonators, Nat. Commun., 9(1), 3283 (2018).
[7] A. T.-H. Lin, J. Yan, A. A. Seshia, Electrically addressed dual resonator sensing platform for biochemical detection, J. Microelectromech. Syst., 21(1), 34-43 (2011).
[8] P. S. Waggoner, H. G. Craighead, Micro- and nanomechanical sensors for environmental, chemical, and biological detection, Lab on a Chip, 7(10), 1238–1255 (2007).
[9] N. E. Weckman, A. A. Seshia, Reducing dissipation in piezoelectric flexural microplate resonators in liquid environments, Sens. Actuators A: Phys., 267, 464-473 (2017).
[10] V. Qaradaghi, A. Ramezany, S. Babu, et al., Nanoelectromechanical disk resonators as highly sensitive mass sensors, IEEE Electron Device Lett., 39(11), 1744-1747 (2018).
[11] U. Schmid and M. Schneider, High Performance Piezoelectric Aln Mems Resonators for Liquid Sensing and Beyond-The Potential of Piezomems, 2019 20th International Conference on Solid-State Sensors, Actuators and Microsystems & Eurosensors XXXIII (TRANSDUCERS & EUROSENSORS XXXIII), 653-654 (2019).
[12] H. Begum, J. Qian, J. E.-Y. Lee, Effect of crystal orientation on liquid phase performance of piezoelectric-on-silicon elliptical plate resonators, Sens. Actuators A: Phys., 340, 113548 (2020).
[13] Z. W. Lin, C. Y. Wu and S. S. Li, Feedthrough Engineering to Enable Resonant Sensors Working in Conductive Medium for Bio Applications, J. Microelectromech. Syst., 33(3), 333-341 (2024).
[14] S. Bhattacharya, S.-S. Li, A fully differential SOI-MEMS thermal piezoresistive ring oscillator in liquid environment intended for mass sensing, IEEE Sens. J., 17,

7261-7268 (2019).
[15] V. Qaradaghi, B. Dousti, Y. Choi, G. S. Lee, W. Hu, S. Pourkamali, Surface area enhancement of nanomechanical disk resonators using MWCNT for mass-sensing applications, IEEE Trans. Ultrason. Ferroelectr. Freq. Control, 66, 609-615 (2019).
[16] Q. Yang, S. Pan, Y. Zhao, H. Zhang, W. Pang, X. Duan, Biomolecular stiffness detection based on positive frequency shift of CMOS compatible gigahertz solidly mounted resonators, Biosen. Bioelectro., 96, 206-212 (2017).
[17] F. Patocka, C. Schneidhofer, N. Dörr, M. Schneider, U. Schmid, Novel resonant MEMS sensor for the detection of particles with dielectric properties in aged lubricating oils, Sens. Actuators A: Phys., 315, 112290 (2020).
[18] E. A. Corbin, L. J. Millet, K. R. Keller, W. P. King, R. Bashir, Measuring physical properties of neuronal and glial cells with resonant microsensors, Anal. Chem., 86, 4864-4872 (2014).
[19] A. K. Bryan, A. Goranov, A. Amon, S. R. Manalis, Measurement of mass, density, and volume during the cell cycle of yeast, PNAS, 107, 999-1004 (2010).
[20] T. P. Burg, M. Godin, S. M. Knudsen, W. Shen, G. Carlson, J. S. Foster, K. Babcock, S. R. Manalis, Weighing of biomolecules, single cells and single nanoparticles in fluid, Nature, 446, 1066-1069 (2007).
[21] M. M. Daryani, T. M., J. Wei, M. K. Ghatkesar, Measuring nanoparticles in liquid with attogram resolution using a microfabricated glass suspended microchannel resonator, Microsyst. Nanoeng., 8(1), 92 (2022).
[22] R. M. R. Pinto, V. Chu and J. P. Conde, Label-Free Biosensing of DNA in Microfluidics Using Amorphous Silicon Capacitive Micro-Cantilevers, IEEE Sens. J., 20(16), 9018-9028 (2020).
[23] N.W. Ombati, T. Kahmann, T. Viereck, E. Peiner, MEMS-based cantilever sensor for simultaneous measurement of mass and magnetic moment of magnetic particles, Chemosensors, 9(8), 207 (2021).
[24] M. Wu, A. Ozcelik, J. Rufo, Z. Wang, R. Fang, T. J. Huang, Acoustofluidic separation of cells and particles, Microsyst. Nanoeng., 5, 32 (2019).
[25] Y. Gu, C. Chen, J. Rufo, C. Shen, Z. Wang, P.-H. Huang, H. Fu, P. Zhang, S. Cummer, Z. Tian, T. J. Huang, Acoustofluidic holography for micro- to nano- scale particle manipulation, ACS Nano, 14, 14635-14645 (2020).
[26] J. Qian, H. Begum, J. E.-Y. Lee, Acoustofluidic localization of sparse particles on a piezoelectric resonant sensor for nanogram-scale mass measurements, Microsyst. Nanoeng., 7, 61 (2021).
[27] J. Qian, H. Begum and J. E.-Y. Lee, Acoustic Centrifugation Facilitating Particle Sensing in Liquid on a Piezoelectric Resonator, IEEE Electron Device Letters, 43, 5, 801-804 (2022).
[28] C. Y. Cheng, A. Dangi, L. Ren, et al., Thin film PZT-based PMUT arrays for deterministic particle manipulation, IEEE Trans. Ultrason. Ferroelectr. Freq.

Control, 66(10), 1606-1615 (2019).
[29] P. Vachon, S. Merugu, J. Sharma, et al., Microfabricated acoustofluidic membrane acoustic waveguide actuator for highly localized in-droplet dynamic particle manipulation, Lab on a Chip, 23(7), 1865-1878 (2023).
[30] H. Begum, J. Qian, and J. E.-Y. Lee, Fully differential higher order transverse mode piezoelectric membrane resonators for enhanced liquid phase quality factors, J. Micromech. Microeng., 31(10), 104004 (2021).
[31] J. Arcamone, E. Colinet, A. Niel, et al., Efficient capacitive transduction of high-frequency micromechanical resonators by intrinsic cancellation of parasitic feedthrough capacitances, App. Phys. Lett., 97(4) (2010).
[32] R. Abdolvand, B. Bahreyni, J. E.-Y. Lee, et al. Micromachined resonators: A review. Micromachines, 7(9),160 (2016).
[33] Y. Bourquin, A. Syed, J. Reboud, et al., Rare-cell enrichment by a rapid, label-free, ultrasonic isopycnic technique for medical diagnostics, Angew. Chem. Int. Ed., 53(22), 5587-5590 (2014).
[34] C. Samarasekera, J. G.W. Sun, Z. Zheng, et al., Trapping, separating, and palpating microbead clusters in droplets and flows using capacitive micromachined ultrasonic transducers (CMUTs), Sens. Actuators B: Chem., 276, 481-488 (2018).
[35] J. Qian, W. Huang, R. Yang, et al., Low-cost laser-cut patterned chips for acoustic concentration of micro-to nanoparticles and cells by operating over a wide frequency range, Analyst, 146(10), 3280-3288 (2021).
[36] P. G. C. Petean, M. L. Aguiar, Determining the adhesion force between particles and rough surfaces, Powder Technol., 274, 67-76 (2015).
[37] S. Rajupet, M. Sow, D. J. Lacks, Particle adhesion to rough surfaces, Phys. Rev. E, 102(1), 012904 (2020).
[38] H. Jia, P. X.-L. Feng, Very high-frequency silicon carbide microdisk resonators with multimode responses in water for particle sensing, J. Microelectromech. Syst., 28, 941-953 (2019).
[39] B. Kim, R. N. Candler, M. Hopcroft, et al., Frequency stability of wafer-scale encapsulated MEMS resonators, The 13th International Conference on Solid-State Sensors, Actuators and Microsystems, 2005. Digest of Technical Papers. TRANSDUCERS'05. IEEE, 2, 1965-1968 (2005).
[40] J. Xu, E. Cao, M. Fahrbach, V. Agluschewitsch, A. Waag and E. Peiner, Real-Time Operation of Microcantilever-based In-plane Resonators Partially Immersed in a Microfluidic Sampler, IEEE Micro Electro Mechanical Systems, 1037-1040 (2023).
[41] S. Bhattacharya, N.-Y. Teng, J. Satija, C.-T. Lin, S.-S. Li, Detection of polystyrene beads concentration using an SOI-MEMS differential rotational thermal piezoresistive resonator for future label-free biosensing applications, IEEE Sens. J., 21, 21400-21409 (2021).
[42] R. Tao, J. Reboud, H. Torun, et al. Integrating microfluidics and biosensing on a single flexible acoustic device using hybrid modes. Lab on a Chip, 20(5), 1002-

1011 (2020).

[43] H. Begum, A. Ali, J E.-Y. Lee. Mass Sensitivity Measurements of a Novel High Q-Factor Disk Resonator for Liquid-Phase Sensing Applications. 2019 20th International Conference on Solid-State Sensors, Actuators and Microsystems & Eurosensors XXXIII (TRANSDUCERS & EUROSENSORS XXXIII), 1886-1889 (2019).

[44] PiezoMUMPs, MEMSCAP (accessed 2 January 2024); http://www.memscap.com/products/ mumps/piezomumps.